NATURAL LAMINAR FLOW AND AIRPLANE STABILITY AND CONTROL*

C. P. van Dam
Vigyan Research Associates, Inc.
Hampton, Virginia 23665

ABSTRACT

Location and mode of transition from laminar to turbulent boundary-layer flow have a dominant effect on the aerodynamic characteristics of an airfoil section. In this paper, the influences of these parameters on the sectional lift and drag characteristics of three airfoils are examined. Both analytical and experimental results demonstrate that when the boundary-layer transitions near the leading edge as a result of surface roughness, extensive trailing-edge separation of the turbulent boundary layer may occur. If the airfoil has a relatively sharp leading edge, leading-edge stall due to laminar separation can occur after the leading-edge suction peak is formed. These two-dimensional results are used to examine the effects of boundary-layer transition behavior on airplane longitudinal and lateral-directional stability and control.

INTRODUCTION

In recent years, airplane construction materials and fabrication methods have improved greatly, resulting in the production of airframe surfaces which are essentially free of roughness and waviness and which accurately match the design shape. Flight tests (e.g., refs. 1 and 2) have demonstrated that extensive runs of laminar flow can be obtained over the region of favorable pressure gradient on smooth airplane surfaces and provide a significant reduction in profile drag.

The application of natural laminar flow (NLF) to improve airplane speed and range, however, has also resulted in concerns about a new set of problems in airplane handling qualities. In order to exhibit satisfactory handling qualities, an airplane must possess a certain measure of both stability and controllability. Recently, a number of airplane stability and control problems have been encountered due to loss of laminar flow in some composite home-built airplanes and this has resulted in articles such as references 3 and 4. In flight, the loss of laminar flow can be the result of leading-edge surface contamination due to insects or moisture.

The purpose of this paper is to examine the effects of NLF on airplane stability and control. The first part of the paper will discuss the manner in which the aerodynamic characteristics of airfoil sections depend on location and mode of transition from laminar to turbulent boundary-layer flow. In the second part, the influence of airfoil aerodynamic characteristics on airplane longitudinal and lateral-directional stability and control will be discussed.

NOMENCLATURE

b wing span, ft

*This research was conducted under NASA Contract No. NAS1-17797.

C_D	airplane drag coefficient
$C_{D,0}$	airplane zero-lift drag coefficient
C_L	airplane lift coefficient
C_{L_α}	lift-curve slope, deg^{-1} or rad^{-1}
C_m	airplane pitching-moment coefficient
C_{m_q}	variation of pitching-moment coefficient with pitch rate
C_{m_α}	variation of pitching-moment coefficient with angle of attack, deg^{-1} or rad^{-1}
C_n	airplane yawing-moment coefficient
C_{n_β}	variation of yawing-moment coefficient with angle of sideslip, deg^{-1} or rad^{-1}
C_p	pressure coefficient, $(p - p_\infty)/q_\infty$
c	chord length, ft
$\bar{c}$	mean aerodynamic chord, ft
c_d	section drag coefficient
c_ℓ	section lift coefficient
c_{ℓ_α}	section lift-curve slope, deg^{-1} or rad^{-1}
c_m	section pitching-moment coefficient
H	boundary-layer shape parameter, δ^*/θ
I_{yy}	airplane moment of inertia about Y-axis, $slug\text{-}ft^2$
M	Mach number
N	airplane yawing moment, ft-lb
p	static pressure, psf
q	dynamic pressure, psf
R	chord Reynolds number
S	lifting surface reference area, ft^2
s	surface length, ft
U_∞	free-stream velocity, ft/sec
V_i	indicated airspeed, knots
v	local velocity, ft/sec
$\bar{X}$	nondimensional longitudinal location, $X/\bar{c}$
x	airfoil abscissa, ft
α	angle of attack, deg
β	angle of sideslip, deg
δ^*	boundary-layer displacement thickness, ft
δ_e	elevator deflection, deg
δ_f	flap deflection, deg
ζ	damping ratio
θ	boundary-layer momentum thickness, ft
ρ	air density, lb/ft^3
ω_n	undamped natural frequency, rad/sec

Subscripts:

ac	aerodynamic center
C	foreplane
cg	center of gravity
max	maximum

P	phugoid mode
SP	short-period mode
t	transition location
WB	wing body
WLT	winglet
∞	free-stream condition

BOUNDARY-LAYER TRANSITION AND AIRFOIL AERODYNAMIC CHARACTERISTICS

The two parameters which have a dominant effect on the aerodynamic characteristics of an airfoil section are boundary-layer transition location and boundary-layer transition mode. The transition modes of most practical interest include transition by inflectional instability at laminar separation or with crossflow vorticity, and transition by viscous (Tollmien-Schlichting) instability.

In most cases, the laminar boundary layer separates quickly when it encounters a slight pressure rise. Boundary-layer transition will take place in the separated boundary layer, and a laminar-separation bubble is formed when the turbulent boundary layer reattaches to the surface. Until recently, it has been assumed that only for Reynolds numbers of less than about 5 million would transition occur at laminar separation. (See e.g., refs. 5 and 6.) However, flight results reported in reference 2 indicate that for surfaces with minimal three-dimensional flow effects, transition occurs downstream of the point of minimum pressure, where laminar separation would be expected, even at relatively large transition Reynolds numbers. An extreme example presented in reference 2 is the case of a high-speed business-jet airplane, where transition has been measured at the 40-percent chord location for a chord Reynolds number of 30 million with the point of minimum pressure located at 35 percent of the chord.

Transition can also take place in the attached boundary layer due to the growth of two-dimensional disturbances in the laminar boundary layer. This growth of the two-dimensional disturbances can be accelerated by surface roughness and waviness. The initial conditions for the turbulent boundary layer which originates in the free-shear layer (due to laminar separation) are quite different as compared to the initial conditions of a turbulent boundary layer which originates in the attached boundary layer.

As mentioned before, transition location is another important parameter when examining the aerodynamic characteristics of an airfoil section. A turbulent boundary layer which originates near an airfoil leading edge produces a very different boundary-layer thickness and profile in the pressure-recovery region than a turbulent boundary layer which originates from transition near the point of minimum pressure. Depending on the pressure distribution in the pressure recovery region, a variation in initial conditions for the turbulent boundary layer can produce turbulent boundary-layer separation and consequently a change in airfoil aerodynamic characteristics. The influence of transition location and transition mode on aerodynamic characteristics can best be demonstrated by examining these characteristics for three airfoil sections.

In figure 1, the geometry and two inviscid velocity distributions for the GU 25-5(11)8 airfoil section are shown. The airfoil section characteristics have been calculated using the low-speed airfoil design and analysis method developed by Eppler and Somers (refs. 7 and 8). The surface pressure can be obtained from the local velocity ratio as follows:

$$C_p = 1 - \left(\frac{v}{U_\infty}\right)^2 \qquad (1)$$

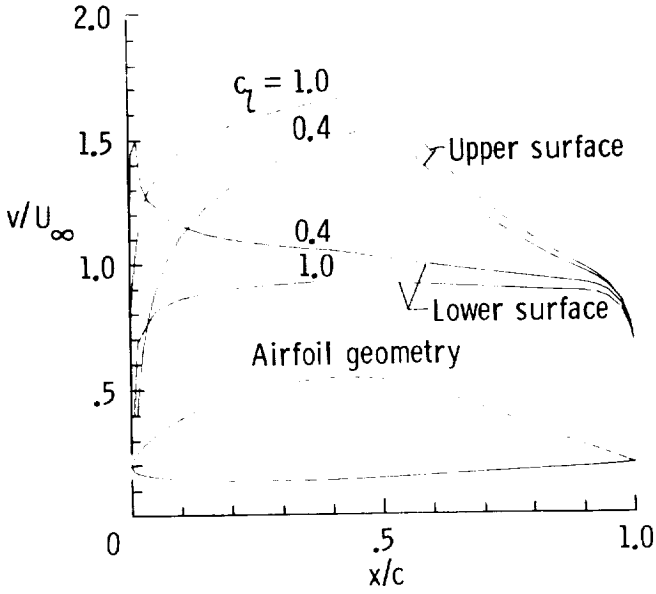

Figure 1.- Geometry and inviscid velocity distributions of GU25-5(11)8 airfoil.

This airfoil section is one of a series of low-drag airfoils designed (ref. 9) and wind-tunnel tested (refs. 10 and 11) at the University of Glasgow during the 1960's. The GU 25-5(11)8 airfoil section has a maximum thickness ratio of 0.20, occurring at 41.6 percent of the chord. The airfoil section is capable of generating a high maximum lift coefficient at relatively low Reynolds numbers. Wind-tunnel data in references 10 and 11 indicate a maximum section lift coefficient of 1.93 at a chord Reynolds number of 0.41 million. Because of these characteristics, a large number of foreplane designs for homebuilt canard configurations have used this airfoil section. The velocity distributions in figure 1 indicate that at approximately 50 percent of the chord the favorable accelerating flow condition over the front portion of the airfoil abruptly changes into an adverse decelerating flow condition over the aft portion of the airfoil. This type of discontinuity in the velocity distribution causes the laminar boundary layer to separate. Transition will occur in the free-shear layer, and the boundary layer will reattach in the form of a turbulent boundary layer.

The main disadvantage of laminar separation in this location will be an increment in section drag. The size of the laminar separation bubble is a function of Reynolds number. With decreasing Reynolds number, the boundary-layer reattachment point moves downstream and the bubble becomes more elongated. Eventually, for a low enough Reynolds number ($R < 200{,}000$ according to ref. 6), reattachment of the turbulent boundary layer will not occur before the trailing edge of the airfoil, and airfoil stall takes place. The results in references 10 and 11 show that in the case of a 12-in.-chord GU 25-5(11)8 airfoil section, a laminar separation bubble of about 1.5-in. length ($x/c = 0.13$) is formed at the onset of pressure recovery at $R = 0.63$ million. In order to eliminate this separation bubble, transition was fixed ahead of the point of minimum pressure by means of a trip wire located at $x/c = 0.455$.

In figure 2, the influence of the laminar separation bubble on the

pressure distribution of the GU 25-5(11)8 is clearly visible. Wortmann (ref. 12) was the first to solve the

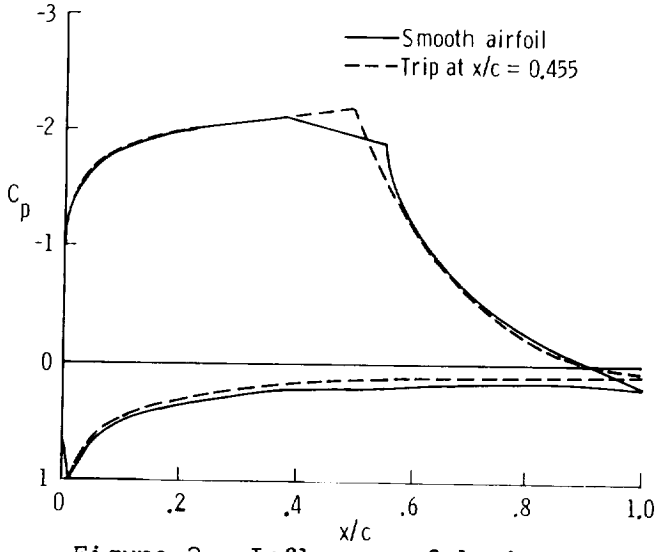

Figure 2.- Influence of laminar separation bubble on pressure distribution of GU 25-5(11)8 at $\alpha = 7.4°$ and R = 0.63 million (ref. 12).

problem of laminar separation bubbles by introducing an instability ramp upstream of the pressure recovery region. The flow condition across the instability ramp is such that the growth of the two-dimensional disturbances in the laminar boundary layer is so strongly accelerated that transition in the attached boundary layer occurs at the end of the instability ramp prior to the steep adverse pressure-gradient flow condition.

Recently, Horstmann and Quast (ref. 6) have introduced pneumatic turbulators to produce premature boundary-layer transition. Small air jets are used to produce highly unstable three-dimensional disturbances in the laminar boundary layer at the onset of the pressure recovery region, thus preventing laminar separation bubbles. An excellent description of the laminar separation bubble and techniques to prevent them are presented in reference 6. With increasing Reynolds number, the size of the laminar separation bubble decreases, and consequently its effect becomes smaller.

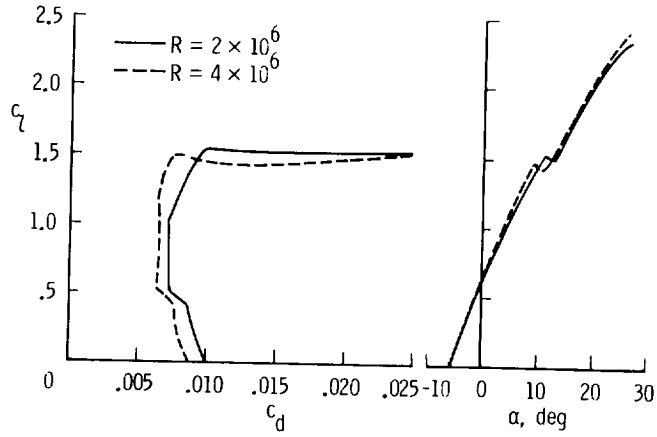

(a) Free transition.

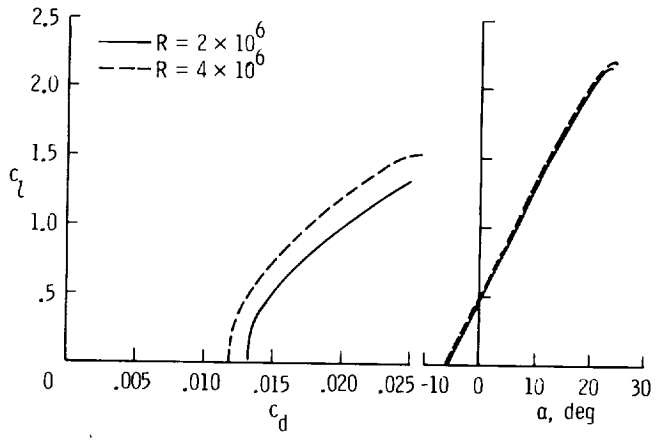

(b) Fixed transition at x/c = 0.075.

Figure 3.- Calculated aerodynamic characteristics of GU 25-5(11)8 airfoil.

In figure 3, the calculated lift and drag characteristics for this airfoil section are presented for R = 2.0 and 4.0 million. In figures 3(a) and 3(b), the results are shown for free boundary-layer transition and fixed transition at x/c = 0.075, respectively. The results for free transition show that airfoil aerodynamic characteristics change dramatically at an angle of attack of approximately

10°. At that angle of attack, a sharp suction peak near the leading edge causes transition to move forward suddenly. Due to this forward shift of transition, trailing-edge separation of the turbulent boundary layer increases, and a loss in lift is encountered. Also, forward movement of transition location and turbulent separation produces a large increment in section drag. The maximum sectional lift coefficients produced by the airfoil are very large in the case of free transition. However, the aerodynamic characteristics change drastically when boundary-layer transition is fixed near the leading edge. The latter simulates the condition when the leading edge of the airfoil section is critically contaminated by insects or moisture. The drag of the GU 25-5(11)8 increases significantly, as expected. However, the lift characteristics of the airfoil section are also affected as is clearly shown in figure 4.

The results in figure 4 indicate that both sectional lift-curve slope, c_{ℓ_α}, and section maximum lift coefficient, $c_{\ell,max}$, are reduced due to fixed boundary-layer transition. Techniques such as instability ramps, trip wires and strips, and pneumatic turbulators have a negligible influence and will not prevent this premature loss in lift when early transition occurs. Much larger devices such as vortex generators are required to prevent or reduce separation of the turbulent boundary layer.

The influence of fixed transition on the boundary-layer development is shown in figure 5. In this figure, nondimensional boundary-layer displacement thickness, δ^*/c, nondimensional boundary-layer momentum thickness, θ/c, and boundary-layer shape factor, $H = \delta^*/\theta$, are plotted as a function of nondimensional distance, s/c, from the stagnation point along the upper

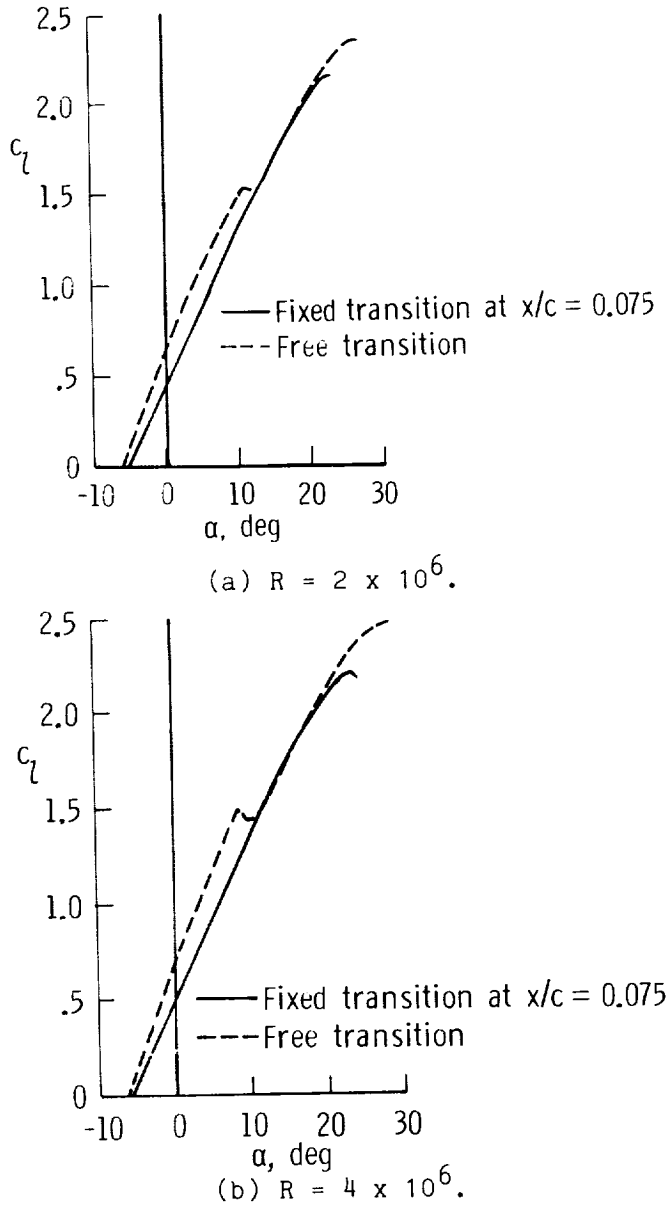

Figure 4.- Influence of transition location on lift characteristics of GU 25-5(11)8 airfoil.

surface of the GU 25-5(11)8 airfoil section at $\alpha = 3°$ and R = 2.0 million. Displacement thickness, δ^*, indicates the distance that the streamlines are displaced from the

surface due to the reduced velocities within the boundary layer. Momentum thickness, θ, is representative of the loss in momentum of the air, $\rho U^2 \theta$, due to the presence of the boundary layer. In figure 5(a), the boundary-layer development is plotted for the case of free transition. Transition occurs at s/c = 0.558 due to laminar separation, and it is followed by a steep drop in the value of H.

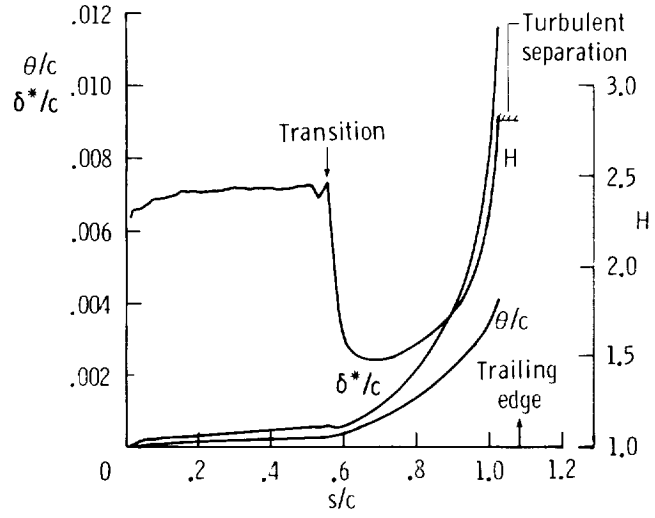

(a) Free transition.

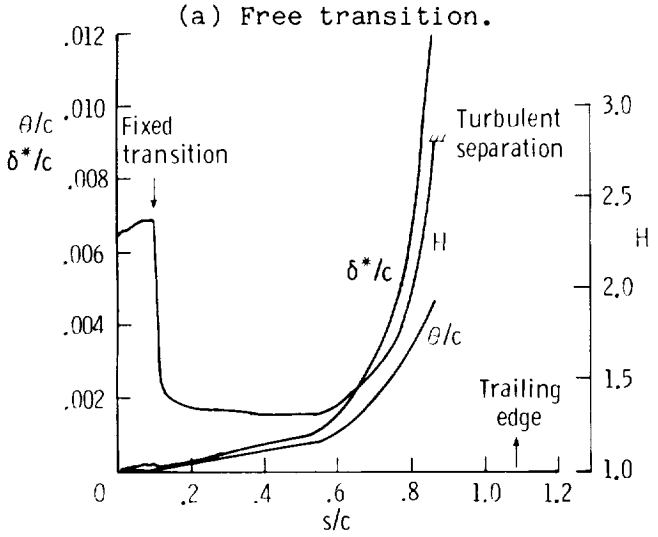

(b) Fixed transition at x/c = 0.075.

Figure 5.- Calculated boundary-layer parameters for upper surface of GU 25-5(11)8 at α = 3° and R = 2 x 10^6.

In the pressure recovery region, displacement thickness and momentum thickness increase rapidly, and turbulent separation is predicted when the boundary-layer shape parameter H reaches a value of 2.8 at s/c = 1.033. In figure 5(b), the boundary-layer development is plotted when transition is fixed at x/c = 0.075 or s/c = 0.116. Downstream of s/c = 0.116, the boundary layer is turbulent, and displacement thickness and momentum thickness grow more rapidly as compared to the laminar case. At the onset of pressure recovery, s/c = 0.524, the displacement thickness and momentum thickness are about 2 to 4 times larger as compared to the laminar case shown in figure 5(a). The steep negative velocity gradient in the pressure recovery region causes these boundary-layer parameters to increase very rapidly resulting in turbulent separation at s/c = 0.873. Thus, for the GU 25-5(11)8 airfoil section, boundary-layer transition near the leading edge results in premature separation of the turbulent boundary layer.

Similar airfoil characteristics have also been shown by Althaus in reference 5. Althaus shows the influence of premature transition caused by leading-edge roughness to be even more

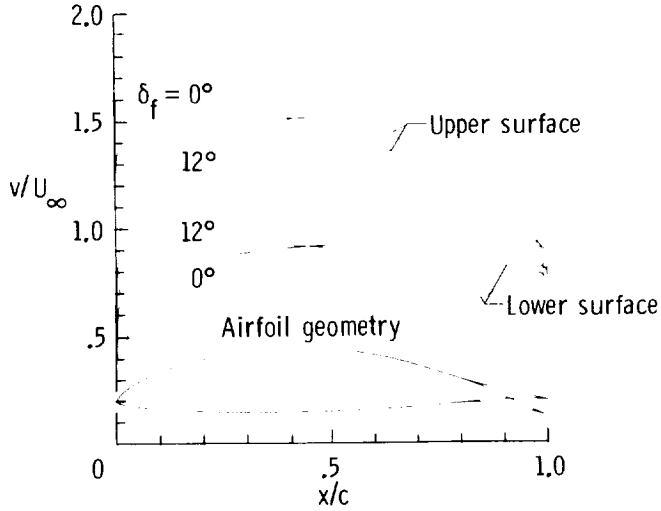

Figure 6.- Geometry and inviscid velocity distributions of FX 67-K-150/17 at c_ℓ = 1.0.

dramatic for certain airfoils with flaps. In figure 6, the geometry and inviscid velocity distribution are shown for the FX 67-K-150/17 airfoil section with and without flap deflection at a constant angle of attack of 9.12° relative to the zero-lift line (inviscid $c_\ell = 1.0$). This airfoil was designed by F. X. Wortmann and wind-tunnel tested by D. Althaus at the University of Stuttgart (ref. 13). The airfoil has a maximum thickness ratio of 15 percent at 40.2 percent of the chord. The flap occupies the final 17 percent of the chord, and the gap between the airfoil and the flap has been sealed. An extensive set of wind-tunnel data for the smooth airfoil is presented in reference 13. Althaus, however, also performed wind-tunnel tests with a simulated pattern for insect debris established on the leading edge. This insect-roughness pattern was simulated by using small pieces of Mylar with bumps which were fastened on the airfoil nose.

Wind-tunnel data for the FX 67-K-150/17 airfoil section with and without his leading-edge roughness pattern are plotted in figure 7. As shown, large changes were measured in the lift and drag characteristics of the airfoil; sectional drag coefficient, c_d, increases while section lift-curve slope, c_{ℓ_α}, decreases significantly due to the loss of NLF. In figure 7(b), the results are shown for a Reynolds number of 1 million and 12° of flap deflection. In addition to the previously mentioned changes in the aerodynamic characteristics of the airfoil, a loss in section maximum lift coefficient can also be noted.

As part of the discussion of the aerodynamic characteristics of the

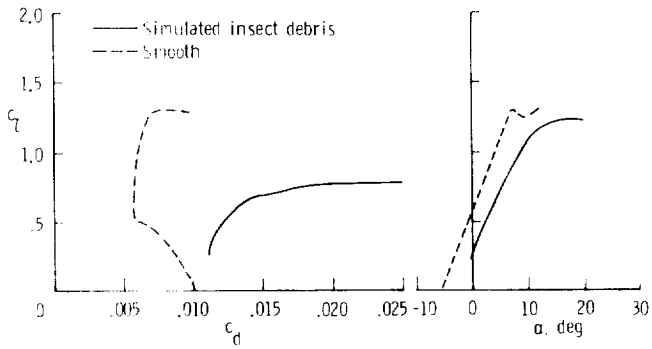

(a) $R = 2.5 \times 10^6$ and $\delta_f = 0°$.

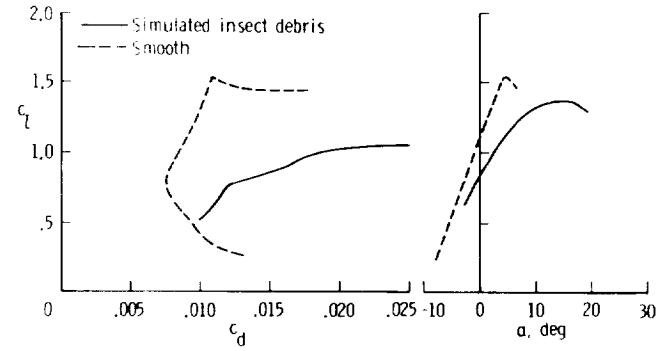

(b) $R = 1 \times 10^6$ and $\delta_f = 12°$.

Figure 7.- Influence of leading-edge contamination on aerodynamic characteristics of FX 67-K-150/17 airfoil (ref. 5).

GU 25-5(11)8 airfoil section, the problem of laminar separation was explained. If the airfoil has a relatively sharp leading edge, however, laminar separation can also occur after the leading-edge suction peak is formed. The laminar boundary layer passes around the leading edge, through the suction peak, and separates. Transition occurs in the separated boundary layer, and initially a laminar separation bubble is formed when the boundary layer reattaches as a turbulent boundary layer. With increasing angle of attack, the suction peak grows rapidly because of high

leading-edge curvature. As a result, the pressure gradient downstream of the point of minimum pressure becomes steeper, and turbulent reattachment becomes more difficult. Sufficient increase in angle of attack can eventually prevent the boundary layer from reattaching to the surface after transition, and leading-edge stall has then occurred. Generally, leading-edge stall is associated with angles of attack larger than those encountered in the cruise flight regime. However, separation near the leading edge can also occur at angles of attack below those encountered in cruise, as will be demonstrated in the following discussion.

Initial airfoil sections recommended for winglet applications on high-speed transport aircraft were developed to operate at supercritical high Mach number design conditions and were cambered to obtain satisfactory high-lift characteristics (ref. 14). In order to avoid producing shock waves on the upper winglet surface and to minimize the added induced velocities on the wing-tip upper surface associated with the winglet, the thickness ratio of the winglet airfoil was held to 8 percent. In a number of cases, subsequent winglet designs for low-speed airplanes have also used this airfoil section. However, this airfoil was not specifically designed for low Reynolds number, low-speed applications, and the airfoil performance under these conditions can be improved.

In figure 8, the airfoil section shape and two inviscid velocity distributions for the original supercritical airfoil are shown. At a cruise lift coefficient of 0.4, the velocity gradient on the upper surface is favorable up to 65 percent of the chord. On the

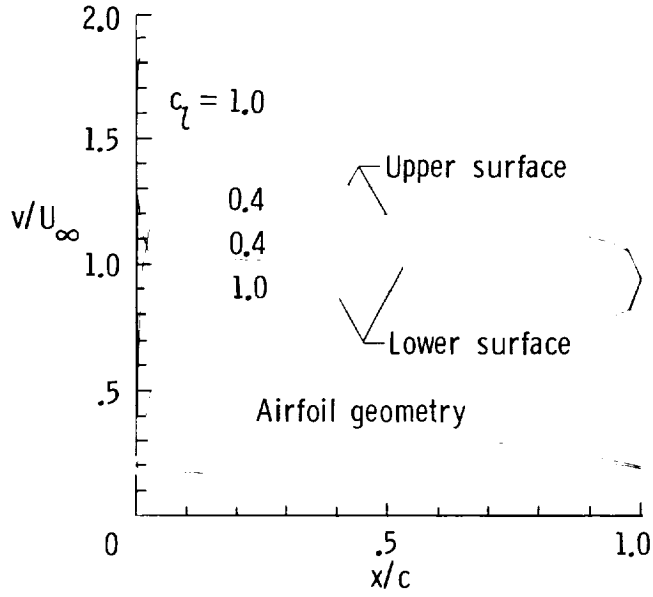

Figure 8.- Geometry and inviscid velocity distributions of supercritical winglet airfoil.

lower surface, however, a sharp suction peak occurs near the leading edge. This suction peak grows with decreasing angle of attack, and the integral boundary-layer method of reference 7 predicts leading-edge flow separation on the lower surface for chord angles of attack lower than approximately -5°. The loss in lift and increment in drag associated with boundary-layer separation can have a significant influence on airplane lateral-directional stability and control. As shown in figure 9, a high maximum sectional lift coefficient is achieved, but the laminar-flow drag bucket is relatively narrow and starts and ends very abruptly. The results also indicate that minimum drag is obtained at a section lift coefficient of 0.6. The combination of a high design lift coefficient and a narrow drag bucket makes this airfoil section less desirable for winglet application on low-speed airplanes. Due to the

shallow pressure recovery, however, section lift characteristics are not influenced by the loss of NLF, as shown in figure 9.

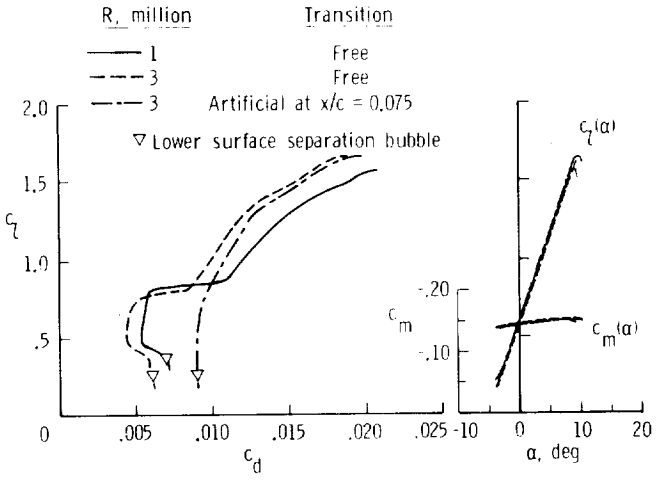

Figure 9.- Calculated aerodynamic characteristics of supercritical winglet airfoil.

The three airfoil sections discussed in this paper should not be viewed as "inferior" or "dangerous" airfoils. These airfoils have been developed with certain design objectives and constraints in mind and are very successful at meeting these design objectives. Airplane designers, however, sometimes select these airfoils to produce lift in operating conditions which violate the original airfoil design conditions.

TRANSITION AND AIRPLANE STABILITY AND CONTROL

In the previous section, the influence of location and mode of transition from laminar to turbulent boundary-layer flow on airfoil aerodynamic characteristics has been discussed. It has been shown that for certain airfoils, if the boundary layer becomes turbulent near the leading edge, extensive trailing-edge separation of the turbulent boundary layer can occur. This boundary-layer separation results in a loss of section lift, and the resulting effects on airplane longitudinal and lateral-directional stability and control characteristics are discussed in the following section. In addition, the influence of winglet airfoil section characteristics on airplane lateral-directional stability and control characteristics is also discussed.

LONGITUDINAL STABILITY AND CONTROL

Generally, longitudinal static stability is required for airplane airworthiness certification. However, too much static stability can have a negative influence on the controllability of an airplane. Dynamic stability is associated with the response behavior of an airplane as a result of a disturbance, and therefore, the damping and frequency of the response motion are examined. Generally, airplanes must also have some form of dynamic stability, i.e., the amplitudes of the motion should diminish progressively as a function of time. Motion damping has a strong effect on airplane handling qualities. If it is too low, then the airplane is too easily excited by disturbances, and if it is too high, then the airplane has a tendency to become too sluggish.

Wind-tunnel experiments have been conducted with the Rutan VariEze. This airplane has a high-aspect-ratio foreplane which uses the GU 25-5(11)8 airfoil section. In references 2 and 15, wind-tunnel data are presented depicting the effect of fixed transition on foreplane lift characteristics and airplane longitudinal aerodynamic characteristics. In the previous

section, it was shown that transition location has a dramatic influence on the lift characteristics of the GU 25-5(11)8 airfoil section. Notably, a loss in section lift-curve slope due to fixed boundary-layer transition was shown (fig. 4). In subsonic flow conditions, the lift-curve slope of the foreplane, $C_{L_{\alpha,C}}$, is a function of the sectional lift-curve slope, c_{ℓ_α}, Mach number, and several planform parameters. Therefore, a reduction in c_{ℓ_α} will reduce the gradient of the foreplane lift curve $C_{L_{\alpha,C}}$.

In figure 10, airplane pitching-moment coefficient, C_m, results clearly demonstrate the large influence of fixed transition on the longitudinal static stability of the airplane.

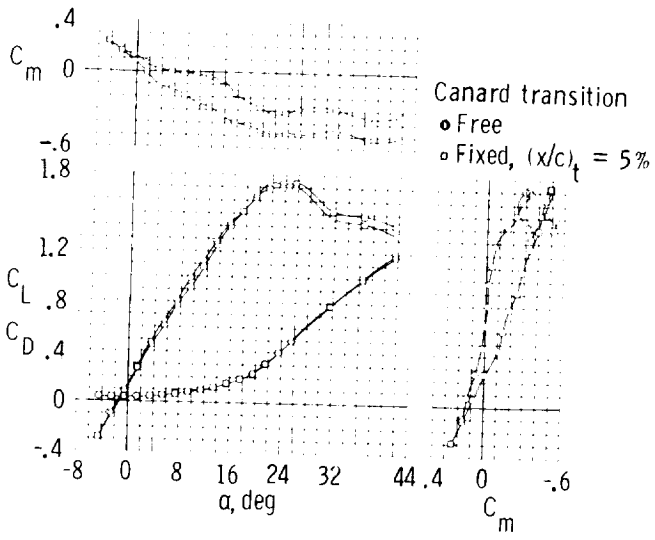

Figure 10.- Longitudinal aerodynamic characteristics of VariEze model as tested in Langley 30- by 60-Foot Tunnel (ref. 2).

For a canard configuration, airplane longitudinal static stability can be written as follows:

$$C_{m_\alpha} = C_{L_{\alpha,C}} \left(\bar{X}_{cg} - \bar{X}_{ac,C}\right) \frac{S_C}{S} + C_{L_{\alpha,WB}} \left(\bar{X}_{cg} - \bar{X}_{ac,WB}\right) \quad (2)$$

where $\bar{X}_{ac,WB} > \bar{X}_{cg} > \bar{X}_{ac,C}$, and $\bar{X}_{cg}$ and $\bar{X}_{ac}$ are defined as the longitudinal location of center of gravity and aerodynamic center, respectively, in terms of airplane mean aerodynamic chord $\bar{c}$. A reduction in $C_{L_{\alpha,C}}$ due to flow separation on the foreplane makes the first term on the right-hand side of equation (2) less positive, and consequently, C_{m_α} becomes more negative. Equation (2) can also be written in the following form:

$$C_{m_\alpha} = C_{L_\alpha} \left(\bar{X}_{cg} - \bar{X}_{ac}\right) \quad (3)$$

where C_{L_α} is defined as airplane lift-curve slope, and $\bar{X}_{ac}$ indicates the longitudinal location of the airplane aerodynamic center in terms of the airplane mean aerodynamic chord. The wind-tunnel results of figure 10 are for a fixed foreplane control surface deflection ($\delta_e = 0°$), and therefore, $\bar{X}_{cg} - \bar{X}_{ac}$ can be defined as stick-fixed static margin of the airplane. The effect of fixed foreplane transition on airplane lift-curve slope is relatively small, as shown in figure 10. In the angle-of-attack range from 3° to 13°, the wind-tunnel data show that airplane static margin (stick fixed) is approximately 0.10 $\bar{c}$ in the case of free transition. When transition is fixed near the leading edge of the foreplane, however, the airplane becomes much more stable and the static margin is approximately 0.30 $\bar{c}$. Thus, airplane aerodynamic center

shifts rearward over a distance of 0.20 $\bar{c}$ as a result of foreplane trailing-edge flow separation.

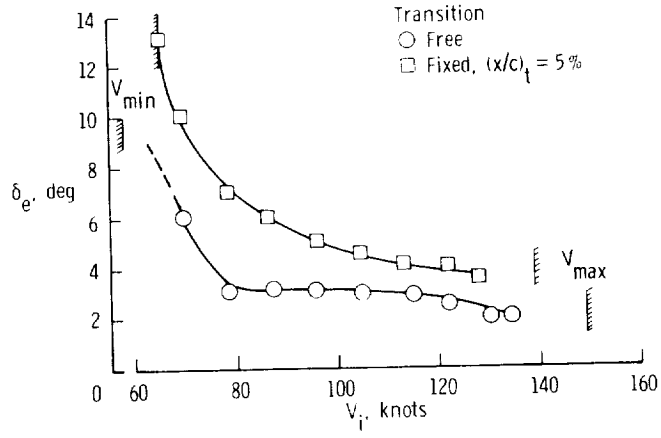

(a) VariEze airplane.

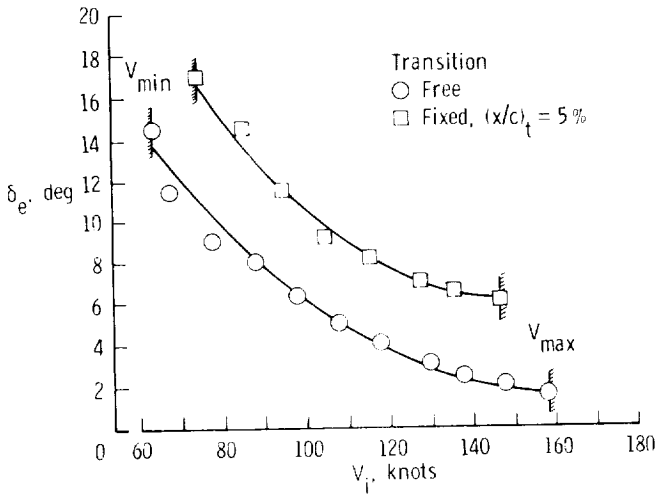

(b) Long-EZ airplane.

Figure 11.- Comparison of fixed versus free transition performance and longitudinal control characteristics as measured in flight (ref. 2).

The wind-tunnel-measured changes in airplane longitudinal aerodynamic characteristics due to fixed transition have also been observed in flight. The original versions of the Rutan VariEze and Long-EZ airplane both use the GU 25-5(11)8 airfoil for the foreplane. Both airplanes have been tested in flight with and without artificial surface roughness near the leading edge of the foreplane in order to measure the changes in airplane longitudinal aerodynamic characteristics caused by loss of NLF. The changes in foreplane lift characteristics with fixed transition come into view when examining elevator deflection required to trim the airplane for a given airspeed, as shown in figure 11. For both airplanes, fixed leading-edge transition induces flow separation on the foreplane, and consequently, increased positive elevator deflection is required to obtain a foreplane lift coefficient which provides longitudinal trim.

In the case of a canard configuration, the influence of wing lift characteristics on the longitudinal static stability is opposite as compared to the influence of foreplane lift characteristics. Therefore, selection of a wing airfoil section shape with lift characteristics which are affected by transition location will result in reduced longitudinal static stability of the airplane. The longitudinal stability and control of both the Rutan VariEze and Long-EZ airplanes appear to be almost unaffected by wing boundary-layer transition location.

For the VariEze and Long-EZ airplanes, the effect of fixed transition on airplane lift-curve slope is shown in figure 12. For both airplanes, the gradient of the lift-curve slope becomes less steep by 7 to 13 percent (ref. 2). The wind-tunnel results, however, only indicate a reduction in lift-curve slope of less than 4 percent. The reason for this

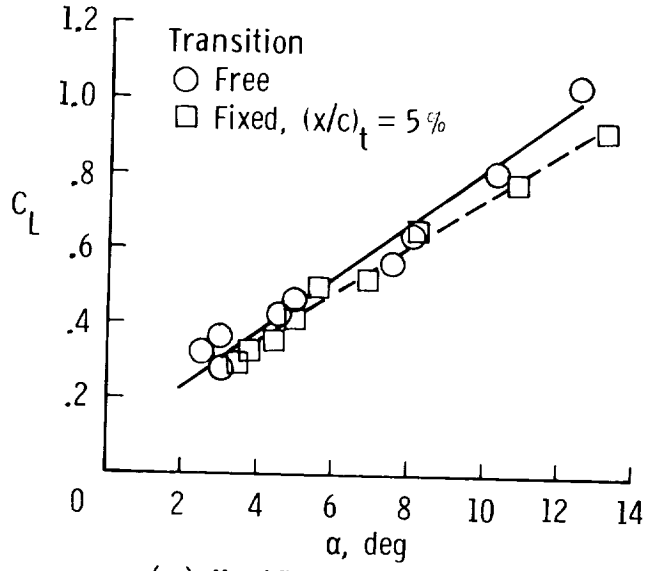

(a) VariEze airplane.

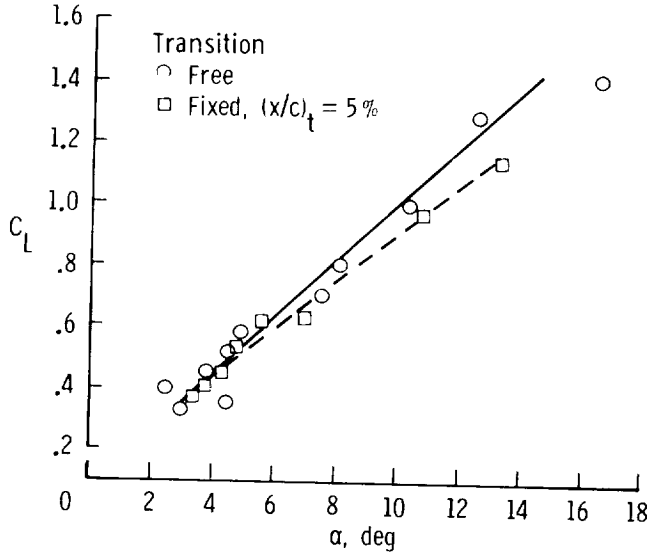

(b) Long-EZ airplane.

Figure 12.- Effect of fixed versus free transition on airplane lift-curve slope as measured in flight (ref. 2).

discrepancy is that the wind-tunnel data of figure 10 have been obtained for a constant elevator deflection $\delta_e = 0°$, while the flight data of figure 12 have been obtained for elevator deflections required to trim the airplane. In flight, lower airspeed results in higher airplane lift coefficient, and therefore, more positive elevator deflection is required for airplane trim, as shown in figure 11. Apparently, trailing-edge flow separation increases with increasing elevator deflection, and consequently the lift loss is augmented at higher airplane lift coefficients. A second contributing factor is the influence of Reynolds number. Flight data at high lift coefficients are obtained at relatively low Reynolds numbers as compared to the Reynolds numbers encountered at low lift coefficients. The following expression depicts this effect more clearly:

$$\frac{R_1}{R_2} = \frac{C_{L_2}}{C_{L_1}} \qquad (4)$$

where it has been assumed that airplane weight and flight altitude are constant and R defines chord Reynolds number. The reduced Reynolds numbers at higher lift coefficients enhance the foreplane separation problem.

The previous results demonstrate the influence of premature boundary-layer separation on airplane longitudinal trim requirements and stick-fixed neutral point location (center-of-gravity location at which $C_{m_\alpha} = 0$). Stick-fixed maneuvering margin is larger than stick-fixed static margin, and the difference between neutral point and maneuver point is proportional to the pitch-damping stability derivative, C_{m_q}. Therefore, if pitch damping is zero, then the difference between neutral point and maneuver point is zero. In the case of canard and conventional configurations, reduced gradients of the lift curve due to flow separation of airplane wing and/or tail will reduce airplane pitch damping and, consequently, reduce the

effects are assumed to be negligible, then phugoid-damping ratio can be

reducing lift-induced drag. The design

difference between stick-fixed static margin and stick-fixed maneuvering margin.

Generally, longitudinal transient behavior of an airplane. According to reference 16, the undamped natural frequency of the short period, $\omega_{n_{SP}}$, is approximately proportional to $\sqrt{-C_{m_\alpha}/I_y}$ where I_y defines the

airplanes have used the airfoil section shown in figure 8. As mentioned previously, this airfoil was developed for winglet application at supercritical, high Mach number conditions. Further, attack and therefore decreased c_ℓ (point C) for the downwind winglet. For the airfoil of figure 8, section drag at the onset of the drag bucket changes rapidly and abruptly. A

ination and leading-edge separation of the laminar boundary layer due to the suction peak have a detrimental effect on airplane stability and controllability. Therefore, for horizontal lifting surfaces such as fore-and tailplanes and wings it is essential to design airfoil section shapes which are not susceptible to boundary-layer separation if no laminar flow exists from the leading edge. For vertical lifting surfaces such as winglets which provide directional stability, an additional design requirement is that transition location on the upper and lower surface should move slowly and steadily with changing angle of attack. The examples given illustrate the importance of proper care in the selection of NLF airfoil characteristics to preclude difficulties with airplane stability and control changes due to the loss of laminar flow.

REFERENCES

1. Holmes, B. J.; Obara, C. J.; Gregorek, G. M.; Hoffman, M. J.; and Freuhler, R. J.: Flight Investigation of Natural Laminar Flow on the Bellanca Skyrocket. SAE paper 830717, April 1983.

2. Holmes, B. J.; Obara, C. J.; and Yip, L. P.: Natural Laminar Flow Experiments on Modern Airplane Sur-

5. Althaus, D.: Influencing Transition on Airfoils. Technical Soaring, December 1981, pp. 82-93.

6. Horstmann, K. H.; and Quast, A.: Drag Reduction by Means of Pneumatic Turbulators. European Space Agency Technical Translation 743, September 1982.

7. Eppler, R.; and Somers, D. M.: A Computer Program for the Design and Analysis of Low-Speed Airfoils. NASA TM-80210, 1980.

8. Eppler, R.; and Somers, D. M.: Supplement to a Computer Program for the Design and Analysis of Low-Speed Airfoils. NASA TM-81862, December 1980.

9. Nonweiler, T.: A New Series of Low-Drag Aerofoils. University of Glasgow, Department of Aeronautics and Fluid Mechanics, Report No. 6801, 1968.

10. Kelling, F. H.: Experimental Investigation of a High-Lift Low-Drag Aerofoil. Aeronautical Research Council Current Papers 1187, 1971.

11. Kelling, F. H.: Experimental Investigation of a High-Lift Low-Drag Aerofoil. University of Glasgow, Department of Aeronautics and Fluid Mechanics, Report No. 6802, September 1968.

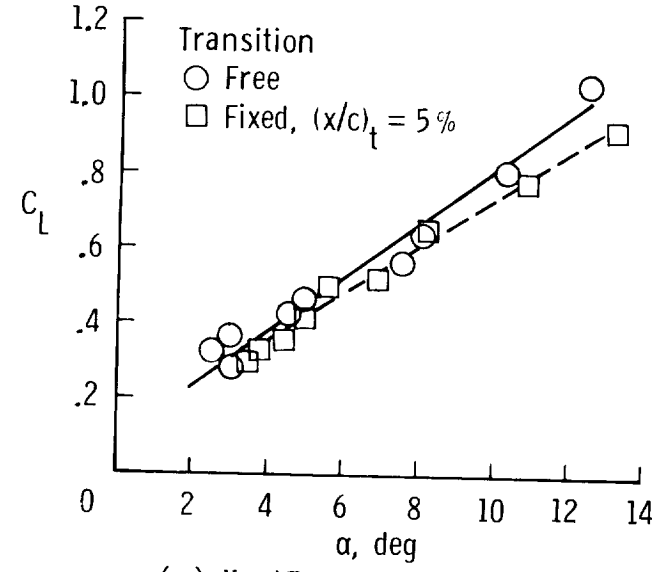

(a) VariEze airplane.

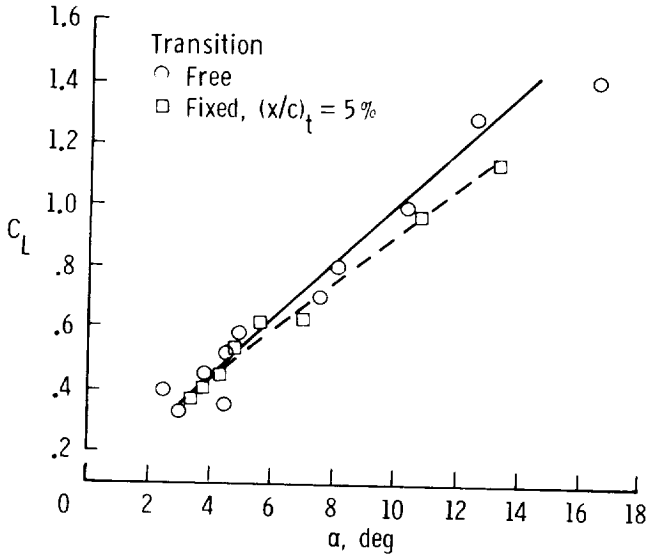

(b) Long-EZ airplane.

Figure 12.- Effect of fixed versus free transition on airplane lift-curve slope as measured in flight (ref. 2).

discrepancy is that the wind-tunnel data of figure 10 have been obtained for a constant elevator deflection $\delta_e = 0°$, while the flight data of figure 12 have been obtained for elevator deflections required to trim the airplane. In flight, lower airspeed results in higher airplane lift coefficient, and therefore, more positive elevator deflection is required for airplane trim, as shown in figure 11. Apparently, trailing-edge flow separation increases with increasing elevator deflection, and consequently the lift loss is augmented at higher airplane lift coefficients. A second contributing factor is the influence of Reynolds number. Flight data at high lift coefficients are obtained at relatively low Reynolds numbers as compared to the Reynolds numbers encountered at low lift coefficients. The following expression depicts this effect more clearly:

$$\frac{R_1}{R_2} = \frac{C_{L_2}}{C_{L_1}} \qquad (4)$$

where it has been assumed that airplane weight and flight altitude are constant and R defines chord Reynolds number. The reduced Reynolds numbers at higher lift coefficients enhance the foreplane separation problem.

The previous results demonstrate the influence of premature boundary-layer separation on airplane longitudinal trim requirements and stick-fixed neutral point location (center-of-gravity location at which $C_{m_\alpha} = 0$). Stick-fixed maneuvering margin is larger than stick-fixed static margin, and the difference between neutral point and maneuver point is proportional to the pitch-damping stability derivative, C_{m_q}. Therefore, if pitch damping is zero, then the difference between neutral point and maneuver point is zero. In the case of canard and conventional configurations, reduced gradients of the lift curve due to flow separation of airplane wing and/or tail will reduce airplane pitch damping and, consequently, reduce the

difference between stick-fixed static margin and stick-fixed maneuvering margin.

Generally, longitudinal transient airplane response consists of two oscillatory terms. The first oscillatory term is called the short-period mode which is highly damped and has a high frequency. The second term describes a very slowly damped, low frequency oscillation which is called the phugoid mode. In the case of the VariEze, a large change in the variation of pitching-moment coefficient with angle of attack, C_{m_α}, is produced due to premature foreplane separation. This stability derivative has a very strong influence on the longitudinal transient behavior of an airplane. According to reference 16, the undamped natural frequency of the short period, $\omega_{n_{SP}}$, is approximately proportional to $\sqrt{-C_{m_\alpha}/I_{yy}}$ where I_{yy} defines the moment of inertia about the airplane Y-axis. Therefore, the influence of C_{m_α} on the undamped natural frequency can be estimated as follows:

$$\frac{\omega_{n_{SP,1}}}{\omega_{n_{SP,2}}} = \frac{C_{m_{\alpha,1}}}{C_{m_{\alpha,2}}} \qquad (5)$$

Thus, an increase of a factor 3 in the value of C_{m_α}, as observed in figure 10, causes the undamped natural

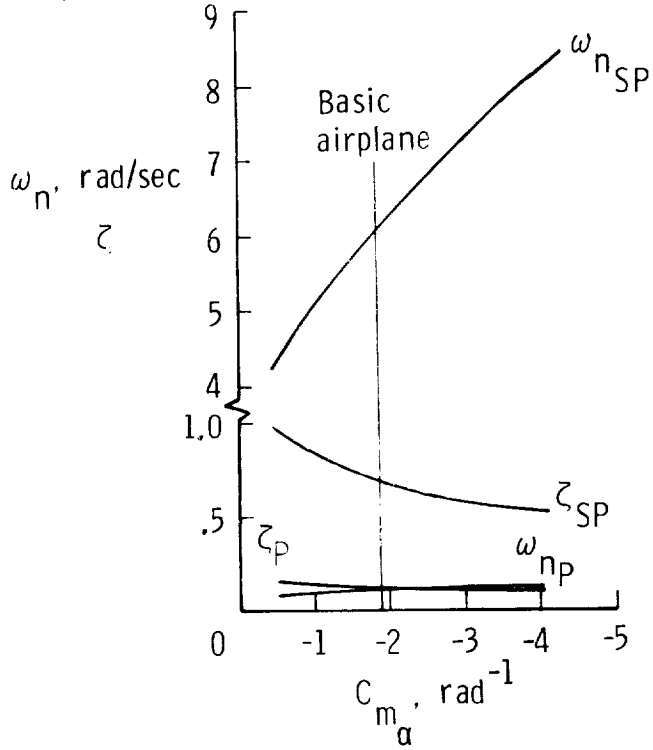

(a) Airplane B at 5,000 ft and M = 0.31.

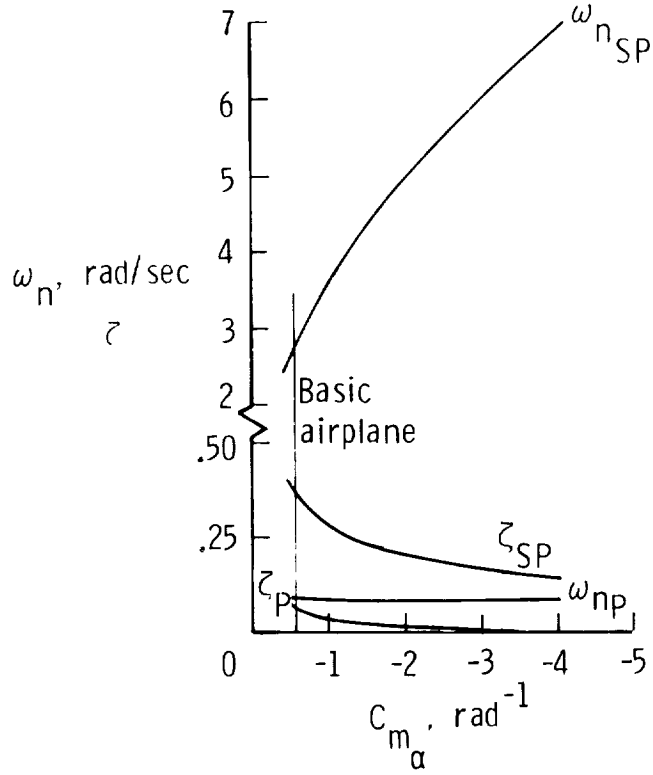

(b) Airplane D at 40,000 ft and M = 0.7.

Figure 13.- Effect of airplane pitching-moment coefficient curve slope on the dynamic stability characteristics.

frequency of the short period to increase by more than 70 percent.

A complete set of stability derivatives was not available for a canard-type airplane. Therefore, a sensitivity analysis was conducted to illustrate the potential influences of $C_{D,0}$ on stability behavior. The results appear in figure 13. The stability derivatives used are presented in reference 16. Airplane B (fig. 13(a)) is representative of Beechcraft B99 type airplanes, while Airplane D (fig. 13(b)) is representative of Gates Learjet Model 24 type airplanes. The results of figure 13 indicate that undamped natural frequency of the short period is strongly influenced by C_{m_α}. Also, short-period damping decreases due to enhanced longitudinal static stability.

As previously mentioned, in general the phugoid mode has a low frequency and is lightly damped. The results in figure 13 verify this statement, and the sensitivity analysis shows that phugoid damping is reduced due to increased longitudinal static stability. This observation matches unpublished flight results obtained with the Rutan Long-EZ by Brown, Holmes, and van Dam. When evaluating airplane handling qualities with fixed foreplane transition, a noticeable reduction in phugoid damping was observed as compared to the phugoid damping with free transition on the foreplane. This effect appears to be more dominant than the influence of airplane drag coefficient on phugoid damping. The latter is sketched in figure 14. If airplane propulsion effects are assumed to be negligible, then phugoid-damping ratio can be approximated as follows (ref. 16):

$$\zeta_P = \frac{C_D}{2\,C_L\sqrt{2}} \qquad (6)$$

According to equation (6), an increase in drag due to transition near the leading edge appears to enhance phugoid damping.

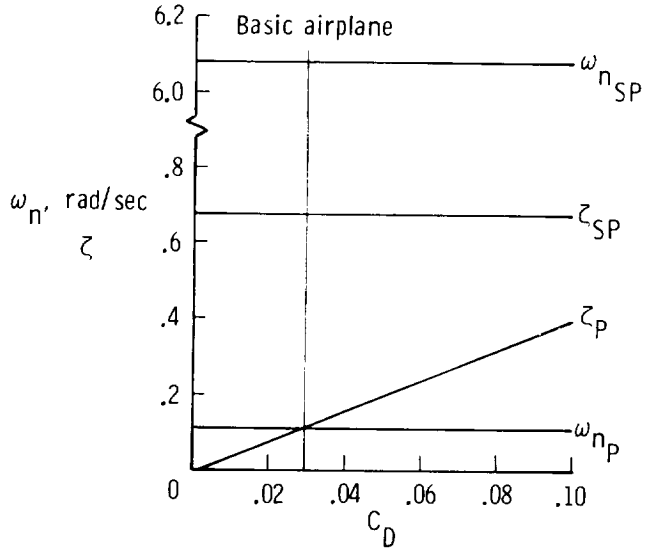

Figure 14.- Effect of airplane drag coefficient on the dynamic longitudinal stability characteristics of airplane B at 5,000 ft and M = 0.31.

Lateral-Directional Stability and Control

Wind-tunnel and flight tests have demonstrated that the use of winglets can provide increased aerodynamic efficiency by reducing lift-induced drag without overly penalizing wing structural weight (ref. 14). A more recent development in the area of airplane design is the utilization of wing-tip-mounted winglets to provide directional stability and control in addition to reducing lift-induced drag. The design of winglet airfoil sections, however, has not received much attention and some winglet designs for low-speed

airplanes have used the airfoil section shown in figure 8. As mentioned previously, this airfoil was developed for winglet application at supercritical, high Mach number conditions. Further, this airfoil was designed with the assumption that the flow over the entire airfoil would be turbulent, primarily as a result of roughness of construction. However, the pressure gradients around $c_\ell = 0.6$ are favorable to NLF as is also indicated by the section drag characteristics in figure 9. The narrow drag bucket is a concern when the winglets also provide directional stability.

The sketch in figure 15 shows the drag polar of the winglet airfoil section and illustrates the potential problem.

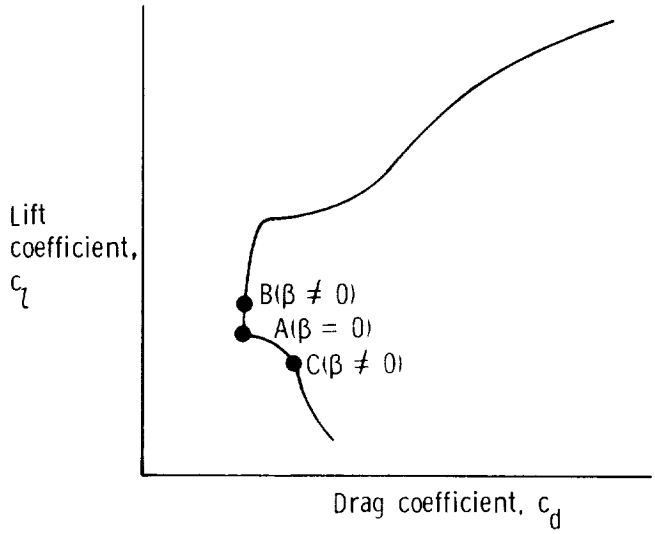

Figure 15.- Drag polar of a winglet airfoil with a sharply defined drag bucket.

Point A in figure 15 indicates the cruise condition at a sideslip angle, β, of 0°. A small positive excursion in sideslip angle causes an increase in angle of attack and as a result enhanced c_ℓ (point B) for the upwind winglet and reduced angle of attack and therefore decreased c_ℓ (point C) for the downwind winglet. For the airfoil of figure 8, section drag at the onset of the drag bucket changes rapidly and abruptly. A significant profile drag differential between the two winglets is produced due to the rapid chordwise movement of boundary-layer transition on the lower surface of the airfoil. This force differential produces a destabilizing yawing moment and can produce undesirable airplane handling qualities. The yawing moment produced by the profile drag differential is ($\beta > 0$)

$$N = - \Delta C_D \, q \, S_{WLT} \, \frac{b}{2} \qquad (7)$$

where S_{WLT} is the area of one winglet and ΔC_D is the profile drag differential between the two winglets. As a result, the change in yawing-moment coefficient is ($\beta > 0$)

$$\Delta C_n = - \frac{\Delta C_D}{4} \Big/ \frac{S_{WLT}}{\frac{S}{2}} \qquad (8)$$

For conventional airplane configurations, the ratio $S_{WLT}/(S/2)$ has a value of 0.02 to 0.10, and as a result, the effect of this destabilizing yawing moment will be small. Some canard configurations, however, use wing-tip-mounted winglets to provide directional stability and control, and because of the relatively short moment arm, the winglet area must be large to provide sufficient directional stability. In that case, $S_{WLT}/(S/2)$ can be larger than 0.20. An area ratio of that value combined with a ΔC_D of about 50 drag counts can generate a destabilizing yawing moment ($\beta > 0$) $\Delta C_n = -0.00025$. This is a relatively small value. However, it may be produced as a result

of a sideslip excursion as small as 0.5°. Therefore, for small sideslip angles, the contribution to the airplane direction stability derivative may be of the order of $\Delta C_{n_\beta} \approx -0.03$ rad^{-1}. This value is large enough to produce significant nonlinearities in the rudder force and rudder deflection variation with sideslip angle.

In order to prevent changes in airplane directional stability, it is important that the lift characteristics of the surfaces which provide directional stability are not affected by premature boundary-layer transition near the leading edge. A reduction in the lift-curve slope of such a lifting surface due to leading-edge roughness will reduce the value of the directional stability derivative C_{n_β} significantly. This derivative has an important influence on the lateral-directional transient response characteristics of the airplane. Generally, all three modes of motion (spiral, roll, and Dutch roll) are affected by a reduction in C_{n_β}. The effects of winglets on the lateral-directional stability characteristics of the Rutan VariEze are clearly depicted in the wind-tunnel results of reference 15 and these results will be used to provide an example. For the angle-of-attack range from 0° to 8°, the destabilizing contribution of the airplane without winglets is $C_{n_\beta} \approx -0.057$ rad^{-1}. In this angle-of-attack range, the winglets produce a $C_{n_{\beta,WLT}} \approx 0.115$ rad^{-1} resulting in an airplane $C_{n_\beta} \approx 0.058$ rad^{-1}. A 10-percent reduction in winglet lift-curve slope due to premature flow separation results in a 10-percent reduction in $C_{n_{\beta,WLT}}$ and a 20-percent reduction in airplane C_{n_β}. The lift characteristics of the VariEze winglets, however, are not sensitive to the transition location from laminar to turbulent boundary layer. Additional information on the design considerations for vertical wing-tip-mounted lifting surfaces on low-speed airplanes is provided in reference 17.

CONCLUSIONS

The analytical and experimental results presented in this paper demonstrate that the location and mode of transition from laminar to turbulent boundary-layer flow can have a significant influence on the lift and drag characteristics of airfoil sections. For airfoils with a relatively steep pressure recovery, it has been shown that boundary-layer transition near the leading edge due to surface contamination can result in trailing-edge separation of the turbulent boundary layer. This premature separation produces a reduction in section lift-curve slope and it can also affect sectional maximum lift coefficient. If the leading edge of the airfoil is relatively sharp, separation of the laminar boundary layer can occur after the leading-edge suction peak is formed. Leading-edge stall arises when the boundary layer after transition does not reattach to the surface.

The two-dimensional results have been used to examine the effects of boundary-layer transition behavior on airplane longitudinal and lateral-directional stability and control. The analyses indicate that both trailing-edge separation of the turbulent boundary layer due to leading-edge contam-

ination and leading-edge separation of the laminar boundary layer due to the suction peak have a detrimental effect on airplane stability and controllability. Therefore, for horizontal lifting surfaces such as fore-and tailplanes and wings it is essential to design airfoil section shapes which are not susceptible to boundary-layer separation if no laminar flow exists from the leading edge. For vertical lifting surfaces such as winglets which provide directional stability, an additional design requirement is that transition location on the upper and lower surface should move slowly and steadily with changing angle of attack. The examples given illustrate the importance of proper care in the selection of NLF airfoil characteristics to preclude difficulties with airplane stability and control changes due to the loss of laminar flow.

REFERENCES

1. Holmes, B. J.; Obara, C. J.; Gregorek, G. M.; Hoffman, M. J.; and Freuhler, R. J.: Flight Investigation of Natural Laminar Flow on the Bellanca Skyrocket. SAE paper 830717, April 1983.

2. Holmes, B. J.; Obara, C. J.; and Yip, L. P.: Natural Laminar Flow Experiments on Modern Airplane Surfaces. NASA TP 2256, June 1984.

3. Dwiggins, D.: Dangerous When Wet?. Homebuilt Aircraft, Part 1 and 2, March and April 1983.

4. Hewes, D.: Effects of Rain and Bugs on Flight Behavior of Tail-First Airplanes. Sport Aviation, Part 1, 2, and 3, May, June, and July 1983.

5. Althaus, D.: Influencing Transition on Airfoils. Technical Soaring, December 1981, pp. 82-93.

6. Horstmann, K. H.; and Quast, A.: Drag Reduction by Means of Pneumatic Turbulators. European Space Agency Technical Translation 743, September 1982.

7. Eppler, R.; and Somers, D. M.: A Computer Program for the Design and Analysis of Low-Speed Airfoils. NASA TM-80210, 1980.

8. Eppler, R.; and Somers, D. M.: Supplement to a Computer Program for the Design and Analysis of Low-Speed Airfoils. NASA TM-81862, December 1980.

9. Nonweiler, T.: A New Series of Low-Drag Aerofoils. University of Glasgow, Department of Aeronautics and Fluid Mechanics, Report No. 6801, 1968.

10. Kelling, F. H.: Experimental Investigation of a High-Lift Low-Drag Aerofoil. Aeronautical Research Council Current Papers 1187, 1971.

11. Kelling, F. H.: Experimental Investigation of a High-Lift Low-Drag Aerofoil. University of Glasgow, Department of Aeronautics and Fluid Mechanics, Report No. 6802, September 1968.

12. Wortmann, F. X.: Experimental Investigation on New Laminar Profiles for Gliders and Helicopters. Ministry of Aviation Translation TIL/T. 4906, 1960.

13. Althaus, D.; and Wortmann, F. X.: Stuttgarter Profilkatalog I, Friedr. Vieweg & Sohn Verlagsgesellschaft mbH, Braunschweig, West Germany, 1981.

14. Whitcomb, Richard T.: A Design Approach and Selected Wind-Tunnel Results at High-Subsonic Speeds for Wing-Tip Mounted Winglets. NASA TN D-8260, July 1976.

15. Yip, Long P.: Wind-Tunnel Investigation of a Full-Scale Canard-Configured General Aviation Airplane. NASA TP 2382, March 1985.

16. Roskam J.: Airplane Flight Dynamics and Automatic Flight Controls. Published by Roskam Aviation Engineering Corporation, 1979.

17. van Dam, C. P.: Natural Laminar Flow Airfoil Design Considerations for Winglets on Low-Speed Airplanes. NASA CR 3853, December 1984.